

Joint Myocardial T_1 and T_2 Mapping Using a Combination of Saturation Recovery and T_2 -preparation

Mehmet Akçakaya,^{1,2,3*} Sebastian Weingärtner,^{3,4} Tamer A. Basha,³ Sébastien Roujol,³ Steven Bellm,³ and Reza Nezafat³

Purpose: To develop a heart-rate independent breath-held joint T_1 – T_2 mapping sequence for accurate simultaneous estimation of coregistered myocardial T_1 and T_2 maps.

Methods: A novel preparation scheme combining both a saturation pulse and T_2 -preparation in a single R–R interval is introduced. The time between these two pulses, as well as the duration of the T_2 -preparation is varied in each heartbeat, acquiring images with different T_1 and T_2 weightings, and no magnetization dependence on previous images. Inherently coregistered T_1 and T_2 maps are calculated from these images. Phantom imaging is performed to compare the proposed maps with spin echo references. In vivo imaging is performed in ten subjects, comparing the accuracy and precision of the proposed technique to existing myocardial T_1 and T_2 mapping sequences of the same duration.

Results: Phantom experiments show that the proposed technique provides accurate quantification of T_1 and T_2 values over a wide-range (T_1 : 260 ms to 1460 ms, T_2 : 40 ms to 200 ms). In vivo imaging shows that the proposed sequence quantifies T_1 and T_2 values similar to a saturation-based T_1 mapping and a conventional breath-hold T_2 mapping sequence, respectively.

Conclusion: The proposed sequence allows joint estimation of accurate and coregistered quantitative myocardial T_1 and T_2 maps in a single breath-hold. **Magn Reson Med 000:000–000, 2015. © 2015 Wiley Periodicals, Inc.**

Key words: quantitative myocardial tissue characterization; myocardial T_1 mapping; myocardial T_2 mapping; myocardial inflammation; diffuse fibrosis

INTRODUCTION

Measurement of the longitudinal (T_1) and the transverse (T_2) relaxation times in the myocardium enables a quantitative description of tissue characteristics and identifi-

cation of various cardiomyopathies. Quantitative myocardial T_1 mapping (1–5) provides a technique for noninvasive assessment of various cardiomyopathies (6) and interstitial diffuse fibrosis (7). When both native and postcontrast myocardial T_1 maps are acquired, they can be used to measure the extracellular volume fraction (8), which has shown utility for detection of diffuse myocardial fibrosis (9). On the other hand, quantitative myocardial T_2 mapping (10–16) enables detection of inflammation and edema (11,14).

Quantitative myocardial mapping approaches rely on acquiring multiple electrocardiogram (ECG)-triggered images with different contrast weightings, achieved by varying one or more sequence parameter(s). Then, a model describing the magnetization evolution, as a function of the unknown parameters of interest and the known sequence parameter(s) that is being varied, is fitted voxel-wise to these series of images.

Several myocardial T_1 mapping approaches have been proposed for sampling of the longitudinal magnetization recovery curve. Look-Locker based inversion-recovery sequences (1,2,17) are commonly used (18–22), with a breath-hold acquisition of each slice, and provide high precision, albeit at the cost of accuracy (5,23). Recently, an inversion-recovery based multislice T_1 mapping sequence has been proposed as well (24). As an alternative to the inversion-based sequences, saturation-recovery based myocardial T_1 mapping was also investigated (25), which was recently revisited by introduction of the SATuration recovery single-SHOT Acquisition sequence (SASHA) (3). Another saturation-recovery based approach called SAPHIRE uses a combination of saturation and inversion pulses (4). These latter techniques have better accuracy compared with Look-Locker based sequences, although their precision tends to be worse (23).

For myocardial T_2 mapping (10–16), several images are acquired with different T_2 -weightings to generate a quantitative pixel-wise T_2 map. T_2 -preparation (T_2 prep) (26) technique has been used to generate these varying T_2 -weighted contrast. Multiple heart-beat rest periods are used in between these images to ensure sufficient magnetization recovery (11,14). An alternative technique, which eliminates the necessity for rest period was recently proposed (27). In this technique, a saturation pulse is used at every R–R interval, followed by a fixed T_1 recovery period. After this recovery, T_2 prep with different echo times are applied to generate a variety of T_2 weighted images, which are acquired immediately afterward. The fixed T_1 recovery period ensures that all the images have the same longitudinal magnetization before

¹Department of Electrical and Computer Engineering, University of Minnesota, Minneapolis, Minnesota, USA.

²Center for Magnetic Resonance Research, University of Minnesota, Minneapolis, Minnesota, USA.

³Department of Medicine, Beth Israel Deaconess Medical Center and Harvard Medical School, Boston, Massachusetts, USA.

⁴Computer Assisted Clinical Medicine, University Medical Center Mannheim, Heidelberg University, Mannheim, Germany

Grant sponsor: NIH; Grant numbers: K99HL111410-01; R00HL111410-03; R01EB008743-01A2; Grant sponsor: Samsung Electronics.

*Correspondence to: Mehmet Akçakaya, Ph.D., University of Minnesota, 200 Union Street S.E., Minneapolis, MN, 55455. E-mail: akcakaya@umn.edu

Received 24 April 2015; revised 14 August 2015; accepted 17 August 2015
DOI 10.1002/mrm.25975

Published online 00 Month 2015 in Wiley Online Library (wileyonlinelibrary.com).

© 2015 Wiley Periodicals, Inc.

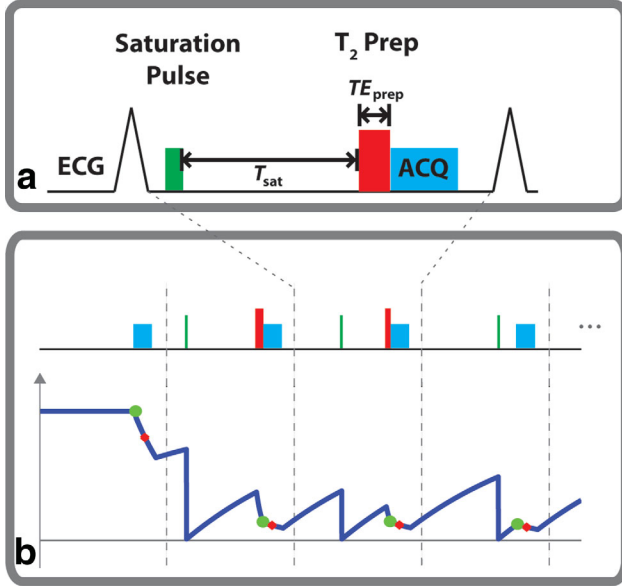


FIG. 1. a: The sequence diagram. A saturation pulse is applied in every R-R interval to eliminate the magnetization history. Following T_1 -based recovery for a duration of T_{sat} , a T_2 -prep with echo length TE_{prep} is applied to generate the additional T_2 weighting, after which a single-shot bSSFP image is acquired. b: The mapping sequence acquires the first image with no magnetization preparation (corresponding to $T_{sat} = \infty$ and $TE_{prep} = 0$), followed by 12 images (3 are shown) acquired with different T_{sat} and TE_{prep} values. The major characteristics of the longitudinal magnetization signal curve are depicted under the pulse sequence diagram. The green circles indicate the magnetization at the end of the preparation pulses, whereas the red circles depict the magnetization when the k-space center is acquired, showing the effect of the bSSFP imaging pulses.

the application of the T_2 prep, and eliminates the need for rest periods, albeit at the cost of a reduced signal-to-noise ratio (27).

Because T_1 and T_2 values offer complementary information, a method for simultaneously mapping these quantities in a reduced amount of time is attractive. Furthermore, the inherently coregistered maps can potentially allow for better visualization of areas with abnormal T_1 or T_2 (28–30). These sequences use different combinations of inversion recovery and T_2 prep techniques to generate different T_1 - and T_2 -weighted images for quantification.

In this study, we sought to develop a saturation-recovery and T_2 -preparation based sequence that exhibits no heart-rate dependence, that can be acquired in a single breath-hold and that allows for accurate simultaneous estimation of myocardial T_1 and T_2 with a precision comparable to existing methods.

METHODS

Proposed Sequence

In the proposed sequence, a saturation pulse is applied to eliminate the magnetization history at every heartbeat. The longitudinal magnetization then recovers based on the T_1 value for a duration of T_{sat} . Subsequently, a T_2 prep pulse (26) with echo length TE_{prep} is applied to

generate the additional T_2 weighting. A single-shot bSSFP image is then acquired using ECG-triggering. The schematic of this proposed joint T_1/T_2 mapping sequence is depicted in Figure 1a. 4 heartbeats of the sequence diagram are shown in Figure 1b, along with the corresponding longitudinal relaxation curve. The longitudinal relaxation curve depicts the effects of the T_1 - T_2 preparations, depicted by the green circles, as well as the imaging pulses, where the red crosses indicate the acquisition of the k-space center. The mapping sequence acquires the first image with no preparation, followed by 12 heartbeats with various (T_{sat}^k, TE_{prep}^k) corresponding to heartbeat k , to sample images with different T_1 and T_2 weightings. These samples were distributed on the two-dimensional grid of possible T_{sat} and TE_{prep} times (31), where the T_{sat} values ranged between 0 and the maximum saturation recovery time within an R-R interval, and TE_{prep} values were limited to a range between 0 and 60 ms.

A composite saturation pulse, based on Sung and Nayak (32), with 1 kHz bandwidth and 10 ms duration is used. T_2 prep uses nonselective opening and closing 90° hard pulses with 2.3 kHz bandwidth and 0.44 ms duration, to minimize T_2^* effects that might occur during the pulse (16), while the refocus pulses are weighted in a MLEV opposing phase pairs scheme to compensate for RF pulse shape imperfection (33). Additionally, for $TE_{prep} = 0$, a 90° followed immediately by a -90° , followed by a crusher gradient was used, similar to the one proposed in Huang et al (10), shown to reduce the effect of B_0 and B_1 variations of the excitation and refocusing pulses of the T_2 prep sequence, and improving the T_2 quantification accuracy (16).

Joint T_1 and T_2 Map Reconstruction

The T_1 and T_2 maps are generated jointly by voxel-wise least-squares fitting of the magnetization evolution model to the image intensities. We use a four-parameter model for fitting, which characterizes the effect of the bSSFP imaging pulses that are played until the acquisition of central k-space, on the magnetization measured after the T_1 and T_2 preparation. This model is given by:

$$M_{4\text{-parameter}}(T_{sat}, TE_{T2P}) = A \left(1 - e^{-T_{sat}/T_1} \right) e^{-TE_{T2P}/T_2} + B, \quad [1]$$

where the parameters, A and B do not depend on the saturation time, T_{sat} or the T_2 prep time, TE_{T2P} . As detailed in Akçakaya et al (16), the B parameter captures the effect of the imaging pulses, and is a function of the steady-state magnetization, as well as sequence parameters. The A parameter is a function of the signal at full-recovery, and sequence parameters (flip angle, number of pulses, repetition time, etc).

Phantom Imaging

All imaging was performed on a 1.5 Tesla (T) Philips Achieva (Philips Healthcare, Best, The Netherlands) system using a 32-channel cardiac coil array. Phantom imaging was performed using 14 NiCl₂ doped agarose vials, whose T_1 and T_2 values spanned a range of values

(T_1 : 260 ms to 1460 ms, T_2 : 40 ms to 200 ms). A single-shot ECG-triggered bSSFP sequence with the following parameters was used for the proposed sequence for imaging at a heart-rate of 60 bpm: two-dimensional (2D) single-slice, field of view (FOV)= 280×280 mm², in-plane resolution= 2×2 mm², slice thickness=8 mm, repetition time/echo time (TR/TE)=2.8 ms/1.4 ms, flip angle=70°, 10 linear ramp-up pulses, SENSE rate=2.5, partial Fourier=0.75, acquisition window=121 ms, number of phase encoding lines=43, linear k-space ordering. Furthermore, to establish the experimental heart-rate invariance of the method, the phantom imaging was repeated using the same imaging parameters at heart-rates of 70, 80, 90, and 100 bpm.

Spin-echo sequences were used to measure reference T_1 and T_2 values for each vial. For T_1 values, an inversion spin-echo sequence was used with 16 inversion times between 100 and 3000 ms, as well as a TR/TE=6000 ms/10 ms. For T_2 values, a Carr-Purcell-Meiboom-Gill (CPMG) spin-echo sequence with an echo train length of 32 with TE 10 ms was performed with TR=6000 ms. The scan parameters were: FOV= 240×240 mm², in-plane resolution= 1.25×1.25 mm², slice thickness=4 mm, flip angle=90°. Number of averages=4.

Finally, T_1 mapping was also performed using SASHA T_1 mapping sequence (3) of the same duration, which is a saturation recovery based technique. For comparison T_2 maps, a conventional T_2 mapping sequence was used with 3 T_2 prep echo times (0, 25, 50 ms), whose acquisitions are separated by a 4-s rest period to allow for sufficient recovery, as well as an image acquired immediately after saturation pulse to simulate a very long T_2 prep echo time (i.e., T_2 prep= ∞) (16). The duration of this acquisition was 4 heartbeats plus 8 s of rest period. The same imaging parameters, as the joint T_1/T_2 sequence, were used for the imaging readout in both the SASHA T_1 and the conventional T_2 mapping acquisitions.

In Vivo Imaging

The study was approved by the institutional review board, and written informed consent was acquired before each examination. In a prospective study, ten healthy adult subjects (31 ± 17 years, 4 men) without contraindications to MRI were recruited. For each subject, localizer scouts were acquired to define the mid-ventricular short-axis slice. The mid-ventricular short-axis slice was acquired using the proposed breath-held single-shot ECG-triggered bSSFP sequence with the same parameters as in phantom imaging. The acquisition took 13 heartbeats. Comparison T_1 maps were acquired using the SASHA T_1 mapping sequence of the same duration within a breath-hold; and comparison T_2 maps were acquired using the conventional T_2 mapping sequence within a breath-hold, with the same parameters as in phantom imaging.

T_1 and T_2 Map Analyses

All T_1 and T_2 maps were generated offline by means of a voxel-wise least-squares fitting using a Levenberg-Marquardt optimizer. The four-parameter model of

Eq. [1] was used for the proposed joint mapping sequence. For phantom imaging, reference T_1 times for the inversion-recovery spin-echo sequence was calculated using a 3-parameter inversion-recovery model,

$$M_{3\text{-parameter}}^{\text{IR-SE}}(T_{\text{inv}}) = A \left(1 - 2e^{-T_{\text{inv}}/T_1} \right) + B. \quad [2]$$

The reference phantom T_2 times for the spin-echo sequence was also calculated using a 3-parameter model,

$$M_{3\text{-parameter}}^{T_2}(TE_{T_2P}) = Ae^{-TE_{T_2P}/T_2} + B. \quad [3]$$

Comparison SASHA T_1 maps were generated using a 3-parameter saturation-recovery model:

$$M_{3\text{-parameter}}^{T_1}(T_{\text{sat}}) = A \left(1 - e^{-T_{\text{sat}}/T_1} \right) + B \quad [4]$$

which was shown to capture the effects of the recovery-curve disturbance caused by multiple RF excitations before the k-space center, as well as reducing the susceptibility to magnetization transfer effects (3,34). Comparison conventional T_2 maps were reconstructed using the 3-parameter model in Eq. [3], which captures the effect of imaging pulses before the k-space center, and whose accuracy was shown to be independent of the T_2 prep echo times (16).

A region-of-interest (ROI) analysis was performed for both phantom and in vivo imaging. The mean value and standard deviation in the ROI were recorded for each calculated T_1 and T_2 maps. For phantom imaging, circular ROIs were drawn across each of the 14 vials, starting from the center of the vial and containing ~ 300 pixels. For in vivo imaging, epi- and endocardial contours were drawn manually by two independent experienced readers blinded to the acquisition type for each map. The T_1 and T_2 values were recorded in the septum (example ROIs are depicted in Supporting Figure S1, which is available online), where the segments show the smallest variation in measurements (35,36). Furthermore, a segment-based analysis was also performed to compare the regional variations of the methods. This included the six segments (anterior, anteroseptal, inferoseptal, inferior, inferolateral, anterolateral) for the mid-ventricular short-axis slice. The standard deviations within these regions were assessed as a surrogate for precision.

For phantom imaging, accuracy was assessed by comparing the mean of the vial for the spin echo reference T_1 (respectively T_2) map, and the mean of the vial for the T_1 (respectively T_2) map from the proposed sequence. The null hypotheses that there was no difference in the mean value for a vial in the spin echo reference and in a map generated using the proposed sequence was tested using a paired t-test across all vials. A P value of <0.05 was considered to be significant. Additionally, Bland-Altman analysis was performed to compare the individual reference T_1 (and T_2) values with those calculated from the proposed sequence. The correlation between the estimated T_1 or T_2 times and the heart rate was studied using Pearson's linear correlation coefficient.

For both phantom and in vivo imaging, the proposed method was compared with SASHA T_1 and conventional

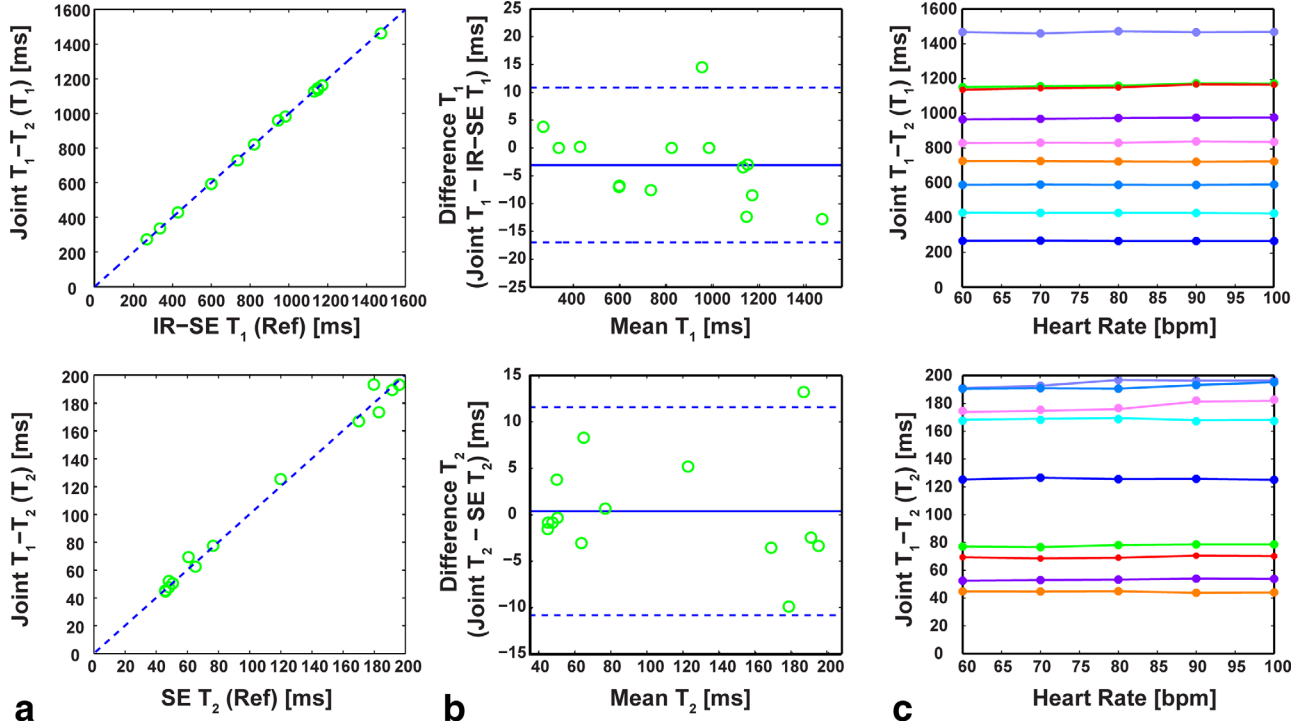


FIG. 2. Phantom results comparing the proposed method to the reference values, as well as showing the heart-rate independence of the method. **a:** T_1 and T_2 (top and bottom rows, respectively) values from the proposed method versus the reference values from the spin echo sequences. The T_1 and T_2 values calculated using the proposed sequence were not different than the reference values ($P=0.49$ in both cases). **b:** Bland-Altman plots comparing the proposed method and reference values, where the variation is within the acceptable range. **c:** The T_1 and T_2 values (top and bottom rows, respectively) in several vials using the proposed sequence for different heart rates, showing no correlation. The vials are color-coded consistently for the T_1 and T_2 graphs.

T_2 mapping, in terms of the measured T_1 or T_2 values, and the associated precision. These values were taken as the average of those of the two independent observers. The null hypotheses that there was no difference in the measured values (or precision) between the maps generated by the proposed T_1 (or T_2) map and the corresponding comparison map were tested using a paired t-test across all vials. A P value of <0.05 was considered to be significant. Bland-Altman analysis was performed to characterize the interobserver variability. Furthermore, Pearson's linear correlation coefficient was used to compare the overall interobserver variability.

RESULTS

Phantom Imaging

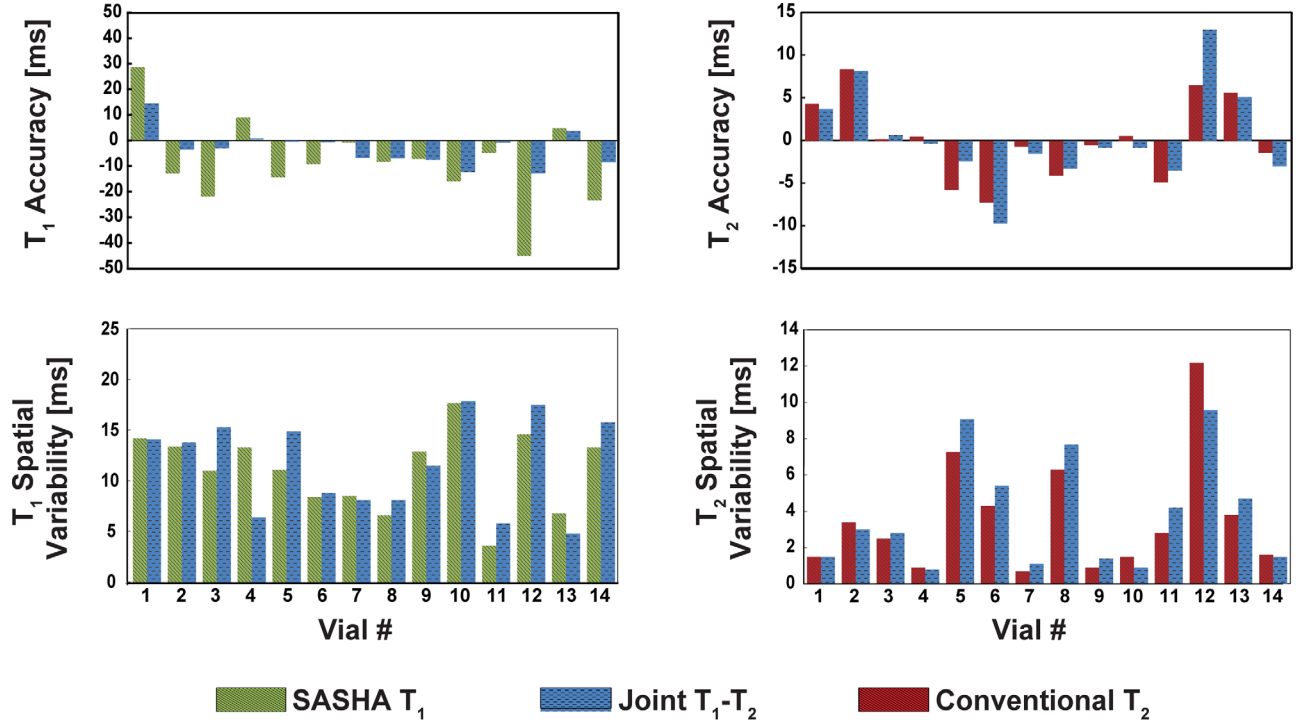
Comparison of the proposed method and the reference values in phantom imaging shows a high level of correlation among the two approaches. The correlation coefficients were 0.99 for both the T_1 and T_2 measurements, and these correlations are depicted in Figure 2a (T_1 in the top, and T_2 in the bottom row, respectively). The T_1 and T_2 values calculated using the proposed sequence were not different than the reference values ($P=0.49$ in both cases). Bland-Altman analysis shows the variation observed between the T_1 and T_2 values (top and bottom rows, respectively) calculated from the proposed method versus the reference values are within the acceptable range (-3.1 ± 13.9 ms for T_1 ; 0.4 ± 11.1 ms for T_2), as

shown in Figure 2b. Finally, the proposed method shows a maximum difference of 1.2% and 2.6% for T_1 and T_2 measurements, respectively, as a function of the heart-rate. There was no significant correlation between the T_1 or T_2 values and the heart-rate, with correlation coefficients <0.2 and $P > 0.95$ for both T_1 and T_2 measurements, demonstrating heart-rate invariance. This heart-rate invariance is depicted in Figure 2c in representative vials for different heart rates for T_1 and T_2 values (top and bottom rows, respectively). The vials are color-coded consistently for the T_1 and T_2 graphs.

Additional comparisons with existing mapping sequences show that for T_1 mapping, both SASHA and proposed T_1 mapping sequences have similar accuracy and precision ($P=0.11$ and 0.34 , respectively). For T_2 mapping, the proposed mapping sequence has similar accuracy and precision compared with the conventional T_2 mapping sequence ($P=0.65$ and 0.36 , respectively). The accuracy and precision for individual vials are depicted in Figure 3.

In Vivo Imaging

The myocardial T_1 and T_2 mapping sequences were successfully completed in all subjects without complications. Example T_1 and T_2 maps from two different subjects are shown in Figure 4, where the maps were of similar visual quality. In both cases there was good agreement of the myocardial T_1 and T_2 values. For subject A, the T_1 and T_2 values were: 1211 ± 82 ms versus



Vial #	1	2	3	4	5	6	7	8	9	10	11	12	13	14
T_1 (ms)	945	1131	1149	336	983	821	600	599	736	1149	428	1476	268	1172
T_2 (ms)	48	61	77	51	192	183	46	196	46	48	170	180	120	65

FIG. 3. Phantom results comparing the proposed method with SASHA T_1 mapping and conventional T_2 mapping of same duration. There was no difference among the corresponding methods in terms of accuracy ($P=0.11$ for T_1 and $P=0.65$ for T_2) or precision ($P=0.34$ for T_1 and $P=0.36$ for T_2). The reference T_1 and T_2 values of the vials from the spin echo sequences are depicted as well.

1210 \pm 92 ms for SASHA and proposed T_1 , respectively; and 49.0 \pm 5.8 ms versus 47.3 \pm 6.5 ms for conventional and proposed T_2 , respectively. For subject B, the T_1 and T_2 values were: 1217 \pm 90 ms versus 1210 \pm 96 ms for SASHA and proposed T_1 ; and 47.8 \pm 7.0 ms versus 45.6 \pm 7.3 ms for conventional and proposed T_2 .

Across all the healthy adult subjects, the estimated ventricular septal T_1 values were: 1210 \pm 24 ms and 1191 \pm 29 ms for SASHA and proposed T_1 mapping, respectively ($P=0.06$). The estimated T_2 values were: 48.2 \pm 2.8 ms and 47.3 \pm 2.3 ms for conventional and proposed T_2 mapping, respectively ($P=0.23$). The measurements for T_1 and T_2 in individual subjects are depicted in Figure 5a. The precision in the septum was: 133 \pm 31.0 ms and 121 \pm 20.7 ms for SASHA and proposed T_1 mapping, respectively ($P=0.08$); and 8.0 \pm 1.2 ms and 9.7 \pm 1.8 ms for conventional and proposed T_2 mapping, respectively ($P=0.01$). The precision for T_1 and T_2 in individual subjects is depicted in Figure 5b. Bland-Altman analysis shows that the interobserver variability was within the acceptable range (-9.6 ± 42.3 ms for T_1 ; 0.7 \pm 5.9 ms for T_2), as depicted in Figure 5c. The correlation coefficient between the two observers for all measurements was 0.99.

The estimated segment-based analysis showed that there was no difference between SASHA and proposed

T_1 mapping in terms of the segmental T_1 values ($P=N.S.$ for all), except for the inferolateral segment (1226 \pm 37.3 ms versus 1198 \pm 37.6 ms, $P=0.01$). There was no difference in terms of the segmental T_1 precision between the two methods across all segments ($P=N.S.$ for all). The results of the segment-based T_1 analysis is depicted in Supporting Figure S2a. The segment-based T_2 analysis revealed that there were no difference between the conventional and proposed T_2 mapping across segments in terms of the T_2 values and T_2 precision ($P=N.S.$ for all), except for the anteroseptal segment, where there was a difference for both the T_2 values (46.9 \pm 2.9 ms versus 46.0 \pm 2.9 ms, $P=0.02$) and precision (7.7 \pm 1.6 ms versus 9.1 \pm 1.9 ms, $P<0.01$). The results of the segment-based T_2 analysis is depicted in Supporting Figure S2b. Furthermore, for all methods, there was a loss of precision in the lateral segments compared with the septal segments ($P<0.01$ for all), consistent with previous studies (35).

DISCUSSION

In this study, we developed a sequence for simultaneously estimating coregistered myocardial T_1 and T_2 maps, based on a combination of saturation-recovery and T_2 -preparation pulses. The proposed sequence was acquired in a single breath-hold over 13 heartbeats. In

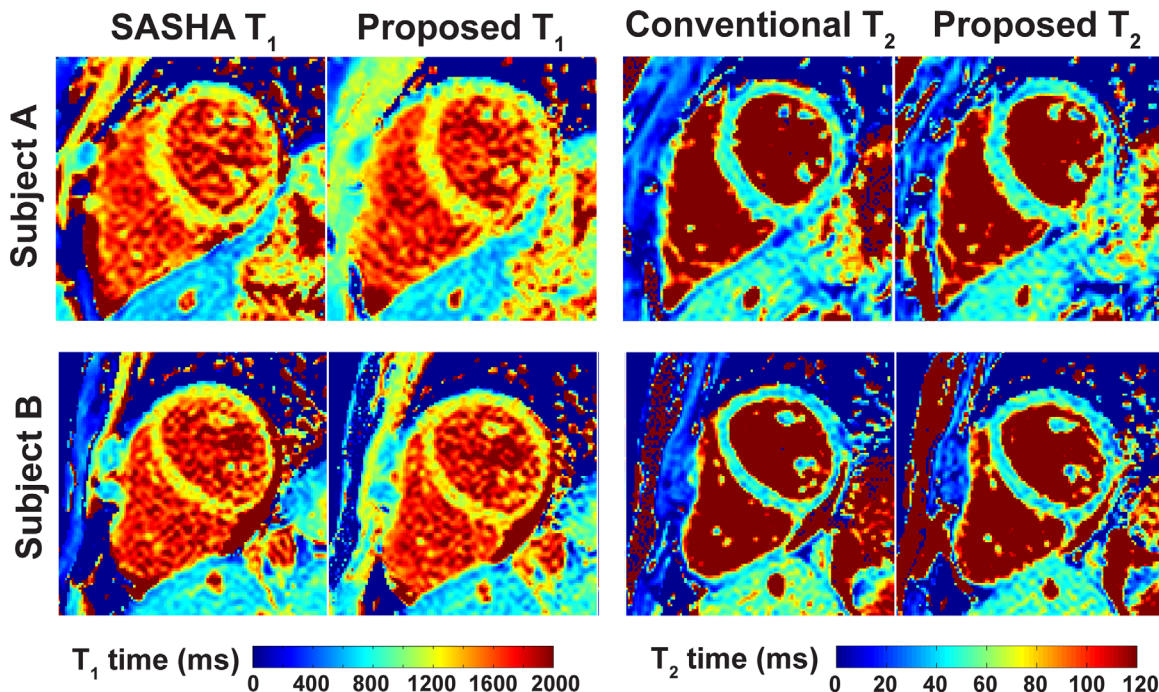


FIG. 4. Example in vivo T_1 and T_2 maps from two different subjects. The maps are visualized with similar quality, and in both cases there was a good agreement of the myocardial T_1 and T_2 values (Subject A: 1211 ± 82 ms versus 1210 ± 92 ms for SASHA and proposed T_1 , respectively; 49.0 ± 5.8 ms and 47.3 ± 6.5 ms for conventional and proposed T_2 , respectively. Subject B, the T_1 and T_2 values were: 1217 ± 90 ms versus 1210 ± 96 ms for SASHA and proposed T_1 ; 47.8 ± 7.0 ms and 45.6 ± 7.3 ms for conventional and proposed T_2).

phantom studies, we established the accuracy of this sequence with respect to spin echo imaging, and also showed that the proposed sequence is heart-rate independent. We also showed that for in vivo data, the quantified septal values were similar to existing methods for individual myocardial T_1 or myocardial T_2 mapping.

In terms of T_1 quantification, the accuracy and precision associated with the proposed method were similar to those of the saturation-recovery based SASHA T_1 mapping. It is understood that SASHA T_1 mapping has better accuracy compared with Look-Locker based sequences, albeit with a degraded precision (23). Because our sequence uses a saturation-recovery approach for generating the T_1 weighting of the individual images, the similarity in characteristics to SASHA sequence is warranted.

For T_2 quantification, the accuracy of the proposed method was similar to a conventional T_2 mapping sequence with four T_2 prep echoes, acquired over 12 s at 60 bpm. The correspondence between these sequences is not straightforward, because the T_2 weighting in the proposed sequence is applied after a saturation recovery pulse (except for the image with no preparation), resulting in a diminished SNR for these images. This seeming disadvantage is mitigated by the ability to acquire an image at every heartbeat due to use of the saturation pulse to erase the magnetization history. On the other hand, the conventional sequence has a higher SNR, but requires multiple rest periods for magnetization regrowth, limiting the number of acquired images. Experimentally, this trade-off offsets the differences, and results in similar accuracy for the proposed sequence, albeit with a reduced precision.

Previous joint T_1/T_2 estimation techniques rely on combinations of inversion recovery and T_2 prep (28–30). In Blume et al (28), a sequence for the simultaneous estimation of T_1 and T_2 maps was proposed using interleaved inversion and T_2 prep pulses. However, this sequence requires multiple relaxation cycles, necessitating a lengthy free-breathing scan, as opposed to a single breath-hold. In Santini et al (29), an alternative joint estimation sequence was proposed based on the inversion-recovery balanced steady-state free-precession (bSSFP) curve. Due to the characteristics of this curve, the estimation is performed sequentially, by first estimating T_1 , and using it to estimate T_2 , as opposed to a simultaneous estimation procedure. Another approach acquires an image with no-preparation, followed by a T_2 -prepared image, and an inversion pulse, after which five images are acquired using a triggered Look-Locker approach (30). These latter sequences can be acquired in a single breath-hold, and were shown to have accuracy similar to MOLLI, which was shown to have lower accuracy compared with saturation-recovery based T_1 mapping sequences (23).

Nulling of the magnetization after the saturation pulse is essential for the performance of saturation recovery based mapping technique. Both composite and adiabatic saturation pulses have been shown to provide robust saturation in cardiac applications (32). Optimization of saturation pulses for myocardial mapping applications is an ongoing area of research (37), and these can be implemented into the current sequence in a straightforward manner. For saturation recovery techniques, it is important to note that in the low SNR regime, the noise in the

This study has several limitations. Only a small number of healthy subjects were recruited. Further clinical evaluations on larger cohorts are warranted to quantify changes in T_1 and T_2 relaxation times in different populations using the proposed method. No validation of the T_1 or T_2 values has been performed in vivo, because a reference time cannot be assessed in the myocardium in a reasonable scan time. Only a single mid-ventricular short-axis slice was imaged in this study. In the proposed approach, a saturation recovery pulse is used at every heartbeat, leading to lower SNR in the individual images, which translates to signal inhomogeneity and spatial variability in the T_1 and T_2 maps. The manual segmentation for the measurements in this study avoided high levels of signal inhomogeneity and contamination. This approach might not be adequate in patients with truly inhomogeneous myocardium, which may limit the application of this technique to diverse patient populations.

CONCLUSIONS

The proposed sequence allows for simultaneous estimation of accurate and coregistered quantitative myocardial T_1 and T_2 maps, without exhibiting heart-rate dependence. It has similar accuracy compared with existing T_1 and T_2 maps sequences of the same duration, and has similar precision for T_1 mapping, albeit having reduced precision for T_2 mapping. Hence, the proposed method enables accurate simultaneous T_1 and T_2 quantification in half the scan time.

REFERENCES

- Messroghli DR, Radjenovic A, Kozierke S, Higgins DM, Sivananthan MU, Ridgway JP. Modified Look-Locker inversion recovery (MOLLI) for high-resolution T_1 mapping of the heart. *Magn Reson Med* 2004; 52:141–146.
- Piechnik SK, Ferreira VM, Dall'Armellina E, Cochlin LE, Greiser A, Neubauer S, Robson MD. Shortened Modified Look-Locker Inversion recovery (ShMOLLI) for clinical myocardial T_1 -mapping at 1.5 and 3 T within a 9 heartbeat breathhold. *J Cardiovasc Magn Reson* 2010;12: 69.
- Chow K, Flewitt JA, Green JD, Pagano JJ, Friedrich MG, Thompson RB. Saturation recovery single-shot acquisition (SASHA) for myocardial T_1 mapping. *Magn Reson Med* 2014;71:2082–2095.
- Weingartner S, Akçakaya M, Basha T, Kissinger KV, Goddu B, Berg S, Manning WJ, Nezafat R. Combined saturation/inversion recovery sequences for improved evaluation of scar and diffuse fibrosis in patients with arrhythmia or heart rate variability. *Magn Reson Med* 2014;71:1024–1034.
- Kellman P, Hansen MS. T_1 -mapping in the heart: accuracy and precision. *J Cardiovasc Magn Reson* 2014;16:2.
- Moon JC, Messroghli DR, Kellman P, et al. Myocardial T_1 mapping and extracellular volume quantification: a Society for Cardiovascular Magnetic Resonance (SCMR) and CMR Working Group of the European Society of Cardiology consensus statement. *J Cardiovasc Magn Reson* 2013;15:92.
- Schulz-Menger J, Friedrich MG. Magnetic resonance imaging in patients with cardiomyopathies: when and why. *Herz* 2000;25:384–391.
- Arheden H, Saeed M, Higgins CB, Gao DW, Bremerich J, Wyttenbach R, Dae MW, Wendland MF. Measurement of the distribution volume of gadopentetate dimeglumine at echo-planar MR imaging to quantify myocardial infarction: comparison with ^{99m}Tc -DTPA autoradiography in rats. *Radiology* 1999;211:698–708.
- Mewton N, Liu CY, Croisille P, Bluemke D, Lima JA. Assessment of myocardial fibrosis with cardiovascular magnetic resonance. *J Am Coll Cardiol* 2011;57:891–903.
- Huang TY, Liu YJ, Stemmer A, Poncelet BP. T_2 measurement of the human myocardium using a T_2 -prepared transient-state TrueFISP sequence. *Magn Reson Med* 2007;57:960–966.
- Giri S, Chung YC, Merchant A, Mihai G, Rajagopalan S, Raman SV, Simonetti OP. T_2 quantification for improved detection of myocardial edema. *J Cardiovasc Magn Reson* 2009;11:56.
- Giri S, Shah S, Xue H, Chung YC, Pennell ML, Guehring J, Zuehlsdorff S, Raman SV, Simonetti OP. Myocardial T_2 mapping with respiratory navigator and automatic nonrigid motion correction. *Magn Reson Med* 2012;68:1570–1578.
- van Heeswijk RB, Feliciano H, Bongard C, Bonanno G, Coppo S, Lauriers N, Locca D, Schwitter J, Stuber M. Free-breathing 3 T magnetic resonance T_2 -mapping of the heart. *JACC Cardiovasc Imaging* 2012;5:1231–1239.
- Verhaert D, Thavendiranathan P, Giri S, Mihai G, Rajagopalan S, Simonetti OP, Raman SV. Direct T_2 quantification of myocardial edema in acute ischemic injury. *JACC Cardiovasc Imaging* 2011;4: 269–278.
- Foltz WD, Al-Kwif O, Sussman MS, Stainsby JA, Wright GA. Optimized spiral imaging for measurement of myocardial T_2 relaxation. *Magn Reson Med* 2003;49:1089–1097.
- Akçakaya M, Basha TA, Weingartner S, Roujol S, Berg S, Nezafat R. Improved quantitative myocardial T_2 mapping: impact of the fitting model. *Magn Reson Med* 2015;74:93–105.
- Kellman P, Arai AE, Xue H. T_1 and extracellular volume mapping in the heart: estimation of error maps and the influence of noise on precision. *J Cardiovasc Magn Reson* 2013;15:56.
- Messroghli DR, Plein S, Higgins DM, Walters K, Jones TR, Ridgway JP, Sivananthan MU. Human myocardium: single-breath-hold MR T_1 mapping with high spatial resolution - reproducibility study. *Radiology* 2006;238:1004–1012.
- Kawel N, Nacif M, Zavodni A, Jones J, Liu S, Sibley C, Bluemke D. T_1 mapping of the myocardium: intra-individual assessment of post-contrast T_1 time evolution and extracellular volume fraction at 3T for Gd-DTPA and Gd-BOPTA. *J Cardiovasc Magn Reson* 2012;14:26.
- Rogers T, Dabir D, Mahmoud I, Voigt T, Schaeffter T, Nagel E, Puntmann VO. Standardization of T_1 measurements with MOLLI in differentiation between health and disease - the ConSept study. *J Cardiovasc Magn Reson* 2013;15:78.
- Raman FS, Kawel-Boehm N, Gai N, Freed M, Han J, Liu CY, Lima JA, Bluemke DA, Liu S. Modified look-locker inversion recovery T_1 mapping indices: assessment of accuracy and reproducibility between magnetic resonance scanners. *J Cardiovasc Magn Reson* 2013;15:64.
- Kellman P, Herzka DA, Arai AE, Hansen MS. Influence of off-resonance in myocardial T_1 -mapping using SSFP based MOLLI method. *J Cardiovasc Magn Reson* 2013;15:63.
- Roujol S, Weingartner S, Foppa M, Chow K, Kawaji K, Ngo LH, Kellman P, Manning WJ, Thompson RB, Nezafat R. Accuracy, precision, and reproducibility of four T_1 mapping sequences: a head-to-head comparison of MOLLI, ShMOLLI, SASHA, and SAPPHERE. *Radiology* 2014;272:683–689.
- Weingartner S, Roujol S, Akçakaya M, Basha TA, Nezafat R. Free-breathing multislice native myocardial T_1 mapping using the slice-interleaved T_1 (STONE) sequence. *Magn Reson Med* 2015;74:115–124.
- Higgins DM, Ridgway JP, Radjenovic A, Sivananthan UM, Smith MA. T_1 measurement using a short acquisition period for quantitative cardiac applications. *Med Phys* 2005;32:1738–1746.
- Brittain JH, Hu BS, Wright GA, Meyer CH, Macovski A, Nishimura DG. Coronary angiography with magnetization-prepared T_2 contrast. *Magn Reson Med* 1995;33:689–696.
- Ding H, Fernandez-de-Manuel L, Schar M, Schuleri KH, Halperin H, He L, Muz Zviman M, Beinart R, Herzka DA. Three-dimensional whole-heart T_2 mapping at 3T. *Magn Reson Med* 2015;74:803–816.
- Blume U, Lockie T, Stehning C, Sinclair S, Uribe S, Razavi R, Schaeffter T. Interleaved $T(1)$ and $T(2)$ relaxation time mapping for cardiac applications. *J Magn Reson Imaging* 2009;29:480–487.
- Santini F, Kawel-Boehm N, Greiser A, Bremerich J, Bieri O. Simultaneous T and T quantification of the myocardium using cardiac balanced-SSFP inversion recovery with interleaved sampling acquisition (CABIRIA). *Magn Reson Med* 2015;74:365–371.
- Kvernbj S, Warntjes MJ, Haraldsson H, Carlhall CJ, Engvall J, Ebbens T. Simultaneous three-dimensional myocardial T_1 and T_2 mapping in one breath hold with 3D-QALAS. *J Cardiovasc Magn Reson* 2014; 16:102.

31. Akçakaya M, Weingärtner S, Roujol S, Nezafat R. On the selection of sampling points for myocardial T_1 mapping. *Magn Reson Med* 2015; 73:1741–1753.
32. Sung K, Nayak KS. Design and use of tailored hard-pulse trains for uniformed saturation of myocardium at 3 Tesla. *Magn Reson Med* 2008;60:997–1002.
33. Levitt M, Freeman R, Frenkiel T. Broadband heteronuclear decoupling. *J Magn Reson* 1982;47:328–330.
34. Robson MD, Piechnik SK, Tunnicliffe EM, Neubauer S. T_1 measurements in the human myocardium: the effects of magnetization transfer on the SASHA and MOLLI sequences. *Magn Reson Med* 2013;70:664–670.
35. Kawel N, Nacif M, Zavodni A, Jones J, Liu S, Sibley CT, Bluemke DA. T_1 mapping of the myocardium: intra-individual assessment of the effect of field strength, cardiac cycle and variation by myocardial region. *J Cardiovasc Magn Reson* 2012;14:27.
36. Puntmann VO, Voigt T, Chen Z, et al. Native T_1 mapping in differentiation of normal myocardium from diffuse disease in hypertrophic and dilated cardiomyopathy. *JACC Cardiovasc Imaging* 2013;6:475–484.
37. Chow K, Kellman P, Spottiswoode BS, Nielles-Vallespin S, Thompson RB. Optimized saturation pulse trains for SASHA T_1 mapping at 3T. *J Cardiovasc Magn Reson* 2015;17(Suppl 1):W20.
38. Roujol S, Foppa M, Weingartner S, Manning WJ, Nezafat R. Adaptive registration of varying contrast-weighted images for improved tissue characterization (ARCTIC): Application to T_1 mapping. *Magn Reson Med* 2015;73:1469–1482.

SUPPORTING INFORMATION

Additional Supporting Information may be found in the online version of this article.

SUP. FIG. S1. Example region of interests (ROIs) segmented for septal analysis of in vivo T_1 and T_2 maps. The ROIs were selected conservatively to avoid signal contamination from the blood pool areas.

SUP. FIG. S2. Summary of the segment-based T_1 and T_2 measurements averaged over all healthy adult subjects, comparing the proposed joint T_1/T_2 method with SASHA T_1 mapping and conventional T_2 mapping of same duration. **a:** The T_1 measurements were statistically similar for all segments ($P = \text{N.S.}$), except the inferolateral segment (1226 ± 37.3 ms versus 1198 ± 37.6 ms, $P = 0.01$). The T_1 precision was similar for all segments ($P = \text{N.S.}$). **b:** T_2 values and T_2 precision were statistically similar for all segments ($P = \text{N.S.}$), except for the anteroseptal segment, where both the T_2 values (46.9 ± 2.9 ms versus 46.0 ± 2.9 ms, $P = 0.02$) and the precision (7.7 ± 1.6 ms versus 9.1 ± 1.9 ms, $P < 0.01$) were different.